Volume 5
Number 7
July 2025
Pages 731–858

Environmental Science Atmospheres

rsc.li/esatmospheres

ISSN 2634-3606

ROYAL SOCIETY OF CHEMISTRY

PAPER
James Allan *et al.*
Quantifying black carbon emissions from traffic and construction in central London using eddy covariance

Environmental Science: Atmospheres

ROYAL SOCIETY OF CHEMISTRY

PAPER

View Article Online
View Journal | View Issue

Open Access Article. Published on 12 May 2025. Downloaded on 1/26/2026 6:50:53 AM.
This article is licensed under a Creative Commons Attribution 3.0 Unported Licence.

Check for updates

Cite this: *Environ. Sci.: Atmos.*, 2025, **5**, 785

Quantifying black carbon emissions from traffic and construction in central London using eddy covariance†

Zixuan Cheng,[a] Dawei Hu,[a] Michael Flynn,[a] Eiko Nemitz,[b] Ben Langford,[b] Will Drysdale,[cd] Carole Helfter,[b] Samuel Cliff,‡[c] Dantong Liu,[e] Rutambhara Joshi,[f] James Cash,[b] James Lee,[cd] Hugh Coe[ag] and James Allan*[ag]

Black carbon (BC) is a significant environmental health and climate forcing concern. Direct measurement of BC fluxes using eddy covariance can quantify emissions and identify sources. Previous studies have examined urban BC emissions in highly polluted countries such as China and India, but to date no equivalent research has been done in the UK and Europe. Here, we present black carbon flux data from a single particle soot photometer (SP2) deployed in an eddy covariance system at the BT (formerly British Telecommunications) Tower in central London. Mean BC mass (number) fluxes with a size range of 60 nm to 600 nm were 6.83 ng m^{-2} s^{-1} (443 cm^{-2} s^{-1}) in summer and 13.3 ng m^{-2} s^{-1} (687 cm^{-2} s^{-1}) in winter, indicating relatively low BC emission when compared to Delhi, which is likely due to the introduction of the ultra-low emission zone (ULEZ) and requirements for road diesel vehicles to meet Euro 6 standards or higher. However, flux footprint analysis identified strong point sources near construction sites during winter and summer observations, which implies that non-road mobile machinery (NRMM) emissions can dominate over traffic BC emissions. This implies that tightened NRMM regulations can help future air quality in London. Observations indicate that the UK's National Atmospheric Emissions Inventory (NAEI) overestimates BC emissions by a factor of 5, although large uncertainties are expected for the combustion sector in the manufacturing industry. The estimate of traffic emissions is more accurate.

Received 1st April 2025
Accepted 9th May 2025

DOI: 10.1039/d5ea00039d

rsc.li/esatmospheres

Environmental significance

Black carbon (BC) has significant health effects, but no direct observations of urban BC emissions have been made in Europe. Quantifying BC emissions and understanding their sources can help make attempts to control BC concentrations and thereby reduce associated health risks. This study presents the first eddy covariance measurement across Europe, highlighting the construction contribution to BC emissions in central London, while inventory overestimates this source by a factor of five. Inventory uncertainties will propagate to models and affect policy decisions. The results also enhance the confidence of BC emissions using eddy covariance by comparing with previous results in Beijing and Delhi. Thus, this study also supports the improvement of air quality management and policy development across different regions.

1 Introduction

Fine particulate matter ($PM_{2.5}$) is a large environmental health concern and results in 4.2 million premature deaths per year.[1] Black carbon (BC) is a carbonaceous material formed by incomplete combustion[2] that comprises an important fraction of $PM_{2.5}$. Epidemiological evidence suggests that BC can cause respiratory diseases, cardiovascular diseases, and adverse effects on the nervous system.[3–5] In densely populated urban areas, people are more likely to be exposed to higher concentrations of BC.[6] Furthermore, BC is second only to greenhouse gases (GHGs) in radiative forcing and warming of the atmosphere *via* the direct absorption of solar radiation.[2] However, unlike GHGs, which mostly have an atmospheric lifetime of

[a]Department of Earth and Environmental Sciences, The University of Manchester, Manchester, M13 9PL, UK. E-mail: James.allan@manchester.ac.uk
[b]UK Centre for Ecology and Hydrology, Bush Estate, Penicuik, EH26 0QB, UK
[c]Wolfson Atmospheric Chemistry Laboratories, Department of Chemistry, University of York, York, YO10 5DD, UK
[d]National Centre for Atmospheric Science, University of York, York, YO10 5DD, UK
[e]Department of Atmospheric Sciences, School of Earth Sciences, Zhejiang University, Hangzhou, Zhejiang, 310027, China
[f]UK Centre for Ecology and Hydrology, Maclean Building, Wallingford, OX10 8BB, UK
[g]National Centre for Atmospheric Science, The University of Manchester, Oxford Road, Manchester, M13 9PL, UK

† Electronic supplementary information (ESI) available. See DOI: https://doi.org/10.1039/d5ea00039d

‡ Now at: Department of Civil and Environmental Engineering, University of California Berkeley, Berkeley, CA 94720, USA.

© 2025 The Author(s). Published by the Royal Society of Chemistry

Open Access Article. Published on 12 May 2025. Downloaded on 1/26/2026 6:50:53 AM. This article is licensed under a Creative Commons Attribution 3.0 Unported Licence.

tens to hundreds of years, the BC lifetime is usually a few days to a week. Therefore, the mitigation of emissions will reap climate benefits on a much faster timescale.[7]

London is the capital city of the UK with a population of 8.8 million and is facing a significant health burden from air pollution that includes the inhalation of BC. To reduce this health burden and meet WHO guidelines for the annual mean of $PM_{2.5} \leq 5$ μg m^{-3}, the world's first ultra-low emission zone (ULEZ) was introduced by the Greater London Authority (GLA) in April 2019 and then expanded to cover all of central London encompassing 4 million people in October 2021. Drivers of motorcycles, petrol vehicles and diesel cars are charged to drive in the ULEZ if they fail to meet Euro 3, Euro 4 and Euro 6 exhaust emission standards, respectively.[8] Of particular note, the requirement for Euro 6 diesel heavy-duty vehicles could have a major impact on $PM_{2.5}$ emissions (g km^{-1}) with a regulatory limit more than 20 times stricter than that of Euro 5. Additionally, the BC fraction within $PM_{2.5}$ is reduced from 75% to 15%.[9] Recent studies suggest that one year after the ULEZ was implemented, nitrogen oxides (NO_x), carbon dioxide (CO_2) and $PM_{2.5}$ emissions within the zone have reduced by 19%, 4% and 7%, respectively.[10]

Atmospheric models are typically used by local governments to estimate and predict the effectiveness of policies. Atmospheric models often use atmospheric inventories as data input.[11] The National Atmospheric Emissions Inventory (NAEI) is a widely used inventory in the UK as the official UK estimate of sources and trends in emissions of air pollutants and greenhouse gases (GHGs).[12] However, atmospheric inventories contain uncertainties caused by (1) the complexity and variability (*e.g.*, temporal and spatial distribution of activities) of emission sources when collecting data, (2) methodological uncertainties in estimation, such as quality control of the mapping approach[13,14] and (3) the complexity of chemistry and meteorological processes, such as those involving NO_x.[11] These uncertainties will propagate to atmospheric models and cause model prediction errors.[15] Therefore, inventory verification is important to ensure inventories correctly represent emissions by sectors. Direct observation of fluxes can enable an evaluation of inventories by comparing the measured fluxes with inventory emission rates as they have the same units and physical meanings.

The eddy covariance (EC) method provides a direct flux measurement for a species of interest that is emitted from or deposited on the surface. In addition, spatial information on emission sources can be obtained *via* flux footprint analysis (FFP). Although more typically used to measure GHG, sensible heat and latent heat exchange of vegetation, the use of EC has expanded to aerosols and variable surfaces including urban environments.[16,17] For example, EC is applied on grassland to measure BC deposition[18] and within urban areas to quantify BC emissions in Beijing and Delhi.[17,19] At the time of writing, no studies have used EC to measure BC emissions within European urban areas.

In this paper, we quantify urban BC emissions in London with an EC system deployed on a 190 meter tower in central London during the summer and winter of 2021. Each season includes a 1 month-long intensive observation campaign. BC concentrations and characteristics were measured using a single particle soot photometer (SP2; Droplet Measurement Technologies, Boulder, USA). Furthermore, FFP analysis was applied to quantify the contribution of BC emissions spatially and identify sources. A comparison between Delhi, Beijing and London was also carried out to initially evaluate differences in BC emissions among cities.

2 Methodology

2.1 Measurement site location

Fluxes of BC were measured intensively in both summer and winter from the BT Tower (51°31′17.4″ N, 0°8′20.04″ W; 190 m) operated by BT GROUP PLC for telecommunications and urban atmospheric pollution observation in central London. The mean building height is 8.8 ± 3 m within 10 km of the BT Tower. Hyde Park and The Regent's Park are located 1.5 km southwest and 1 km northwest, respectively, of the tower. The surrounding area is a high-density human activity zone including busy roads, shopping centres and construction sites.

The EC system at the BT Tower consists of a 3D ultrasonic anemometer (R3-50, Gill Instruments, Lymington, UK) operating at 20 Hz,[20] deployed together with the SP2 sample line inlet as described below. The SP2 was deployed in an air-conditioned room located on the 35th floor of the 44-storey tower, subsampling from a 45 m 1/2″ outside diameter, 3/8″ inside diameter copper tube. The impact and uncertainty caused by the long tube will be discussed in Section 2.4.

2.2 BC measurements and calibrations

Refractory black carbon (rBC) is operationally defined as the BC measured by laser-induced incandescence (LII). The concentrations and physical properties of rBC particles were quantified and characterised using a single particle soot photometer (SP2) based on LII technology.[21,22] The sample flow containing the BC was interacted with an intra-cavity Nd:YAG Gaussian laser beam at 1064 nm pumped by a diode laser inside the SP2 chamber. rBC absorbs laser light and emits incandescent light, while non-rBC materials only scatter the laser light. The emitted and scattered light from individual particles is detected as incandescence and scattering signals by the avalanche photodiode detector (APD) in the optical head of the SP2. Every rBC containing particle, which can trigger incandescence and scattering channels, in the sample flow should be recorded under ideal conditions. However, due to the limitation of hard drive space, the sampling frequency was set to 1 in 3 particles in winter and 1 in 2 particles in summer in this study.

The SP2 can measure ambient BC because 1064 nm light is mainly absorbed by BC in the atmosphere. In this study, quantitative rBC mass concentrations were calculated from the incandescence signal measured by the SP2 based on calibrations with Aqueous Deflocculated Acheson Graphite (Aquadag), a standard BC particle with known size and mass. A correction coefficient of 0.75 was applied to account for the difference in the light absorption of Aquadag compared with ambient BC.[23,24] Number concentrations of rBC containing particles were

 © 2025 The Author(s). Published by the Royal Society of Chemistry

Open Access Article. Published on 12 May 2025. Downloaded on 1/26/2026 6:50:53 AM. This article is licensed under a Creative Commons Attribution 3.0 Unported Licence.

determined directly from the statistics of the incandescence signal.

BC particles can be simulated using the core–shell model, which means a concentric sphere with a BC core and non-BC material around the core, also known as coatings.[25] The BC core diameter (D_c) is converted from rBC mass using BC atmosphere density ($\rho = 1.8$ g cm^{-3}). BC particle size including any coatings is derived from the scattering signal of the SP2. However, coatings of BC particles can vaporize because the laser heats particles, causing a collapse of the scattering signal. The collapse signal can be reconstructed using the scattering signal before vaporization, through what is called a Leading-Edge-Only (LEO) fit.[21,23] The coating of BC is quantified using the scattering enhancement method,[23,26] and the parameter of the scattering enhancement method E_{sca} is defined as eqn (1):

$$E_{sca} = \frac{S_{measured,coated}}{S_{calculated,uncoated}}, \quad (1)$$

where $S_{measured,coated}$ represents the scattering signal of the BC particle with any coatings measured by the SP2 after LEO fitting and scattering channel calibration using polystyrene latex (PSLs; Thermo Fisher Scientific), and $S_{calculated,uncoated}$ is the scattering signal of the corresponding BC core without any coatings, calculated using the BC core refractive index at an SP2 laser wavelength of 1064 nm.[26–28] From this definition, for a given BC core, $E_{sca} = 1$ means no coating, while a larger E_{sca} implies a thicker coating enveloping the BC core.

In this study, the E_{sca} analysis was not applied in the summer campaign because the calibration could not be performed due to Covid restrictions. Aquadag calibrations were conducted in the lab after the summer campaign. Aquadag calibrations in winter were conducted at the Birmingham Air Quality Supersite (BAQS) after the BT Tower campaign, during which a one-month SP2 measurement was undertaken using the same SP2 as in London. Therefore, a PSL calibration with the same SP2 was conducted upon returning to the lab after the winter campaign.

2.3 BC flux calculation

The BC flux (F_{BC}) was derived as the covariance between instantaneous fluctuations of BC concentrations (C'_{BC}) and vertical wind speed (w').[29] The fluctuations were derived by Reynolds decomposition. For example, BC concentration fluctuations can be calculated using eqn (2):

$$C'_{BC} = C_{BC} - \overline{C_{BC}}, \quad (2)$$

where C_{BC} is the BC concentration measured by SP2 at 5 Hz, and $\overline{C_{BC}}$ is the arithmetic mean of C_{BC} over the 30 minute average interval. Then, BC flux can be calculated following eqn (3):

$$F_{BC} = \overline{w' C'_{BC}}, \quad (3)$$

Here, F_{BC} is the BC flux equal to the covariance of BC instantaneous fluctuation (C'_{BC}) and vertical wind speed instantaneous fluctuation (w') over 30 minutes. In the atmosphere, turbulent eddies provide the dominant vertical transport mechanism for most scalars (*e.g.* air pollutant concentrations). The 30 minute average interval is sufficient to capture most eddies and also avoid most non-stationarities during the interval such as synoptic changes.[29–31]

The entities w' and C'_{BC} are recorded with a time lag caused by the 45 m sample line separating the sonic anemometer and SP2, which needs to be removed prior to application of eqn (3). This time lag was estimated by the maximization of covariance method.[16,17] Here, the time lag is calculated every 24 hours in 3 weeks at the beginning, middle and end of each campaign. In this study, the median lag times were 9 s in summer and 7 s in winter.

F_{BC} calculations were performed using EddyPro (version 7.0.6, LI-COR Inc.), open-source software developed for calculating EC fluxes, especially for greenhouse gas (GHG) fluxes. Sonic anemometer data were resampled using trapezoidal average to match the same time resolution (5 Hz) as C_{BC}.

2.4 Corrections and quality control

The EC method requires several assumptions to reduce flux uncertainties and to ensure that the measured flux is representative of the surface exchange.[32,33] The sample inlet is deployed at a height of 190 m, which is more than ten times higher than the urban canopy around it (averaged 12 m). Furthermore, the measurement can represent the area of interest for the prevailing wind directions because of the height. EC assumes that wind speed and scalars are measured in the constant flux layer, where turbulence properties are vertically uniform. However, the BT Tower measurement height may extend above the constant flux layer, which is defined as the lowest 10% of the boundary layer.[34] In such a case, the EC flux would underestimate the surface exchange due to vertical flux divergence (VFD) caused by storage, advection and boundary layer entrainment.[35,36] VFD is a function of measurement heights, constant flux heights and entrainment heights (80% of the boundary layer height). This implies that VFD uncertainty becomes noticeable when measurement heights reach entrainment heights. During both BT Tower campaigns, the boundary layer heights (BLHs) were estimated from the ECMWF reanalysis global meteorology product (ERA5) and corrected using the factor described previously.[36] The BLH diurnal profile (Fig. S6†) shows a mean scaled BLH of around 500 m even in the evening, indicating that entrainment heights are much higher than measurement heights. Applying VFD corrections leads to a 22% (summer) and 15% (winter) increase in the averaged mass fluxes when using ERA5 BLH. If the scaled BLH is used, the increase changes to 21% (summer) and 1% (winter). However, due to the uncertainties in the BLH data and scaling factor (Pearson correlation factor of 0.59 (ref. 36)), applying VFD corrections may introduce additional low frequency error to the total flux. Therefore, VFD corrections were not applied in this study. Nonetheless, we recommend that future studies at the BT Tower include direct BLH measurements, along with a concentration profile between the ground and the observation height. In addition, to ensure horizontal terrain and turbulent flux transformation, we applied (1) tilt corrections, (2) a stationarity

Open Access Article. Published on 12 May 2025. Downloaded on 1/26/2026 6:50:53 AM. This article is licensed under a Creative Commons Attribution 3.0 Unported Licence.

test and (3) a friction velocity test. The EC method also has significant uncertainties at low and high frequencies.[29] Here, we applied spectral analysis to estimate the low and high frequency losses.

2.4.1 Tilt corrections. Tilt corrections allow correcting the measured wind speed to align with the average wind flow line to ensure that the mean value of fluctuations is zero. Double rotation[37] is applied here to each 30 minute data segment to rotate the coordinates to align one wind component (u) with the mean wind flow and nullify the 30 minute means of the cross-wind (v) and vertical (w) wind components.

Eqn (3) in Section 2.3 requires removal of the average of signals from fluctuations under ideal stationary conditions. However, ideal stationary, steady-state conditions are uncommon in the real atmosphere. Linear detrending of each 30 minute interval allows the removal of long term (low frequency) trends from fluctuations, which have no contributions to total fluxes.[38] Here, we applied linear detrending to remove the low frequency trend, which is specifically SP2 BC concentration variation within the 30 minute average interval.

2.4.2 Stationarity and friction velocity corrections. At night, the absence of solar heating impedes turbulence development. This low-turbulence boundary layer at night may induce non-stationarity because advection flow dominates pollutant transport and enables accumulation (storage) of material released from the surface below the measurement. Suppressed vertical mixing increases the flux footprint resulting in measuring fluxes outside the area of interest. These advection processes present challenges to EC measurements, which quantify vertical transport between the surface and the atmosphere. For this reason, fluxes were flagged and filtered based on stationarity tests and friction velocity criteria.

To ensure that 30 minute average intervals meet the assumption of turbulence statistically invariant, we applied a stationarity test[39] in which the 30 minute flux interval was divided into six sub-intervals, and the fluxes of sub-intervals are calculated. The stationarity test compares the 30 minute fluxes with the average of the sub-intervals' fluxes. If the difference exceeded 30%, the 30 minute interval flux was flagged and filtered out. After applying the stationarity test, 10.8% (mass) and 11.6% (number) in summer and 12.7% (mass) and 11.2% (number) in winter data points were removed, and the fluxes increased 7.50% (mass) and 9.00% (number) in summer and 9.90% (mass) and 12.0% (number) in winter.

Friction velocity (u^*) serves as a metric for assessing the vertical transport efficiency of atmospheric turbulence and the pollutants. To ensure that the turbulence is fully developed, the flux intervals with $u^* < 0.2$ m s^{-1} were filtered.[11,30,35,36]

2.4.3 Negative fluxes. In EC measurements, positive fluxes represent net surface-to-atmosphere transport (emission), while negative fluxes indicate the opposite (deposition). To better address that, exchange velocity (V_{ex}) in winter was calculated using $V_{ex} = F_{BC}/\overline{C_{BC}}$ for each 30 minute interval as shown in Fig. S1,† and positive V_{ex} indicates net emission while negative indicates net deposition. Emission and deposition can occur simultaneously over the urban surface.[16] The deposition flux (F_{dep}) can be determined using

$$F_{dep} = -C \times V_d \tag{4}$$

where C is the concentration of interest scalar (BC) and V_d is the corresponding deposition velocity. V_d for BC was observed to be 0.3 ± 0.2 mm s^{-1} over grassland;[18] however, there is no information on BC V_d for urban surfaces. Particles V_d over urban surfaces can be estimated using sulfate (SO_4^{2-}), which is a function of u^*,[16] to be 0 to 3.5 mm s^{-1} for u^* 0 to 1 m s^{-1} which is larger than grassland. This indicates that the morphology of surface elements would affect V_d.[16] So V_d is consistent in a 30 minute interval, while concentration variability can influence the deposition fluxes, potentially exceeding emission and resulting in negative fluxes.

During winter measurements, three periods of sustained negative fluxes were observed (2021/12/18 0:30–2021/12/18 9:00; 2021/12/24 18:00–2021/12/25 8:00; 2021/12/25 18:00–2021/12/26 7:00) after applying the corrections as discussed above. These periods accounted for 4% of the total flux. We noted that there is no distinct spike in BC concentration (Fig. S4†) during these periods, suggesting that the deposition was low. The precipitation washout of BC could have reduced BC concentration, leading to suppressed deposition flux. Neither the double rotation application nor flow distortion could be identified as reasons for the negative flux (Fig. S1 and S2†). Large downward momentum fluxes were observed during these periods (Fig. S1†), suggesting that the reservoir of BC above the measurement height may be responsible for the negative fluxes in this study. To address this, we applied a 24 hour NOAA backward trajectory analysis model to estimate the sources of the BC reservoir (Fig. S3†). Air movements above the measurement height during the negative flux periods are shown to transport from the European continent, possibly due to additional BC emissions related to holiday activities (Christmas). Thus, these negative fluxes were removed from the total fluxes during the deposition period.

2.4.4 Spectral analysis. Mixing in inlet lines results in high-frequency losses in the closed-path EC system, which were evaluated using spectral analysis. This loss greatly increases under laminar flow conditions which therefore need to be avoided.[29] An effective way is to run at high flow rates to avoid laminar flow. Turbulent flow can be quantified *via* the Reynolds number (Re) and the high frequency losses can be corrected according to Re as described previously.[36] Co-spectral density, which indicates the covariance of vertical wind speed (w) and scalar (BC number and mass concentration) in the frequency domain, is calculated using Fast Fourier Transform (FFT). The frequency is normalised by multiplying the measurement height ($z - z_d$; $z_d = 0.67 \times$ canopy height) and then dividing by the wind speed ($f(z - z_d)/u$), which allows the frequency to coincide with the inertial subrange. Co-spectra densities are normalised by multiplying natural frequency and dividing by the covariance flux to bring both co-spectra to approximately the same level. Normalised co-spectra collapse into universal curves allowing the evaluation of the contribution of each frequency band to the total flux. Negative normalised co-spectra mean momentum (w) and scalar (BC) are transported in different directions, indicating a negative contribution to total

 © 2025 The Author(s). Published by the Royal Society of Chemistry

Open Access Article. Published on 12 May 2025. Downloaded on 1/26/2026 6:50:53 AM.
This article is licensed under a Creative Commons Attribution 3.0 Unported Licence.

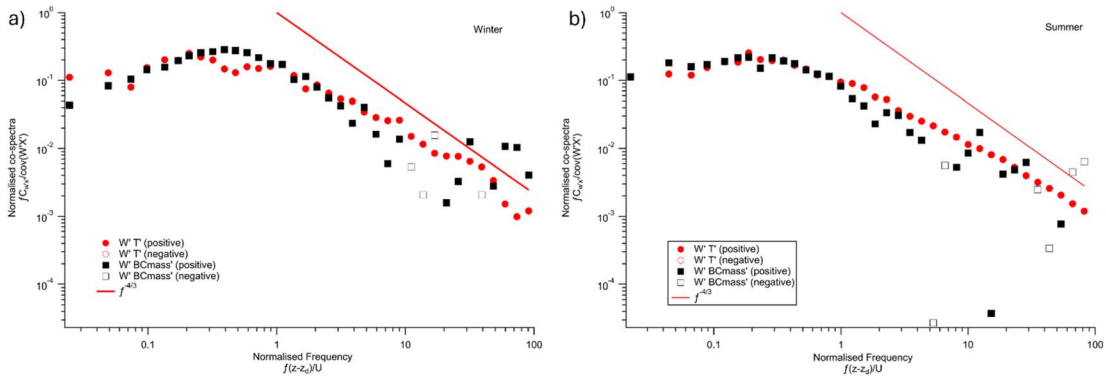

Fig. 1 Co-spectral analysis in winter (194 cases, (a)) and summer (201 cases, (b)) which are binned into 40 evenly spaced bins. BC flux < 0 ng^{-2} s^{-1} and u*< 0.2 m s^{-1} co-spectra are removed. Empty marks indicate negative contribution to total flux and are negated when plotting.

flux. Since sensible heat fluxes (HFs) are measured with a sonic anemometer, which has a higher time resolution and measures at the top of the tower without any tubes, HF spectra are often used as reference spectra.[17,18] Normalised F_{BC} and HF cospectra were compared for both campaigns as shown in Fig. 1. HF co-spectra satisfied the energy cascade ideal $f^{-4/3}$ relationship[40] in the inertial subrange which improves the confidence in using HF cospectra as reference cospectra. In the two seasons, BC exhibits a shape similar to the reference spectrum (HF) across nearly all frequencies, except for losses in the high-frequency range (>10 Hz). To address this high-frequency loss, we applied the ogives analysis,[41,42] which calculates cumulative spectra starting from high frequencies, thus facilitating a more precise evaluation of the high-frequency losses. The difference between the F_{BC} ogive (Fig. 2, black) and HF ogive (Fig. 2, red) is less than 10%. The winter ogive was scaled using a factor of 0.96 resulting in 6.8% flux losses, while the summer ogive was scaled using a factor of 0.90 resulting in 9.9% flux losses, as shown in Fig. S9.† This reflects the large eddy size at the BT Tower height and is consistent with other BT Tower based studies.[30,36] In summary, high-frequency correction was not applied here.

2.5 Footprint modelling

The flux footprint (FFP) refers to the area in the prevailing upwind direction that contributes to the measured fluxes. Here, a parameterized version of the Lagrangian backward model based on EddyPro was applied to determine the distance to the footprint maximum of each 30 minute flux measurement, which represents the location of the maximum contribution to the flux.[43] This footprint maximum is then mapped onto a geographical map using the R-based OpenAir package[44] following an approach as described previously.[36] In short, the approach uses the maximum distance of the footprint to replace wind speed in producing a wind rose plot and maps the plot to geographical coordinates (latitude and longitude).

2.6 NO_x and CO measurements and activity data

Long-term NO and NO_2 measurements using a dual-channel chemiluminescence analyser (Air Quality Design Inc., Boulder, Colorado, USA; 5 Hz) began in September 2020 at the BT Tower,[35,36] whilst long-term CO measurements at the tower were made as part of UKCEH's National Capability programme, historically with an Aerolaser fast CO monitor (model AL5002) at 10 Hz[30] and during these campaigns with a dual quantum cascade laser direct absorption spectrometer (Aerodyne Research Inc., USA). NO_x and CO fluxes were all calculated using the EC method and shared the same ultrasonic anemometer and inlet described in Section 2.1.

Traffic data were from Transport for London (TfL) *via* a freedom-of-information request during the measurement campaigns.[35] The NRMM type, power rating, EU emission standard stage, approval number and exemption covering

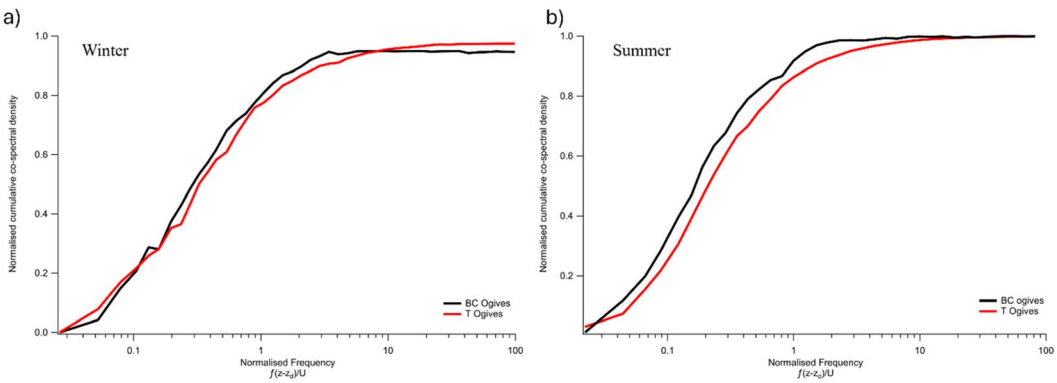

Fig. 2 Normalised cumulative co-spectra (ogives) of BC flux (black) and HF (red) in winter (a) and summer (b).

Open Access Article. Published on 12 May 2025. Downloaded on 1/26/2026 6:50:53 AM.
This article is licensed under a Creative Commons Attribution 3.0 Unported Licence.

footprint area during both campaigns were also provided by the Greater London Authority (GLA) *via* a freedom-of-information request.[45] However, the specific site name was not provided due to data protection regulations.

3 Results and discussion

3.1 BC mixing state

Here, we applied scattering enhancement analysis[17,23,26,28] to characterize the BC mixing state at the BT Tower (Fig. 3). Previous work identifies four distinct mixing states, which were not observed in this study.[28] BC observed at the BT Tower was primarily associated with thinly coated particles (E_{sca} close to 1) across a broad range of BC core diameters (D_c). In contrast to the results for ground based measurement,[23] BC in central London exhibited an absence of larger, thickly coated particles, implying limited biomass burning sources inside the footprint area. However, we cannot assert with complete confidence from E_{sca} analysis that BC concentrations observed in this study are entirely not related to wood burning, as indicated by the success rate in Fig. 3. At the end of the winter campaign, high peak concentrations of BC were identified (Fig. S4†) while ambient temperature and BLH were low, which means that convection can cause BC transport from rural areas, which may include BC from domestic burning sources. However, these BC concentrations have a very limited effect on fluxes because of the low frequency and stable boundary layer corrections.

3.2 Micrometeorological conditions

In EC measurements, u^* not only provides thresholds for advection flux, but also helps us understand the diurnal cycle of turbulence development. The levels and diurnal patterns of u^* during winter (Fig. 4b, blue) and summer (Fig. 4b, yellow) exhibit similarities, suggesting that the measurement height is sufficient to minimize the impact of underlying surface roughness on the measurement results. Sensible heat flux (HF) represents the temperature difference between the upper and lower layers at the measurement site. In both winter (Fig. 4a, yellow) and summer (Fig. 4a, blue), HF increases rapidly after sunrise. This phenomenon is attributed to solar heating of the Earth's surface, leading to an elevation in the temperature of the lower layer. The near negative HF throughout the day in winter occurred due to weaker solar heating, resulting in a slightly higher temperature of the upper layer than the lower layer. Solar heating during summer is more intense than in winter and heats the surface more efficiently, resulting in a greater temperature difference and positive HF.

3.3 BC fluxes

After applying the corrections and filter criteria described above, the remaining mass flux data points comprised of in 919 flux measurements remained for winter (Fig. 5b) and 929 flux measurements for summer (Fig. 5a), each measurement representing a 30 minute interval. Overall, observations were dominated by positive BC fluxes, indicating the presence of anthropogenic activities producing BC emissions.

The average BC fluxes were higher during winter compared to summer (Table 1), which is also evident in the diurnal variation plots (Fig. 5c and f). In both seasons, BC fluxes rapidly increased after sunrise, peaked in the early afternoon, and gradually decreased after sunset. Furthermore, the diurnal patterns were similar between the two seasons, suggesting comparable emission sources for both periods. However, in the morning, summer fluxes rose earlier than in winter due to

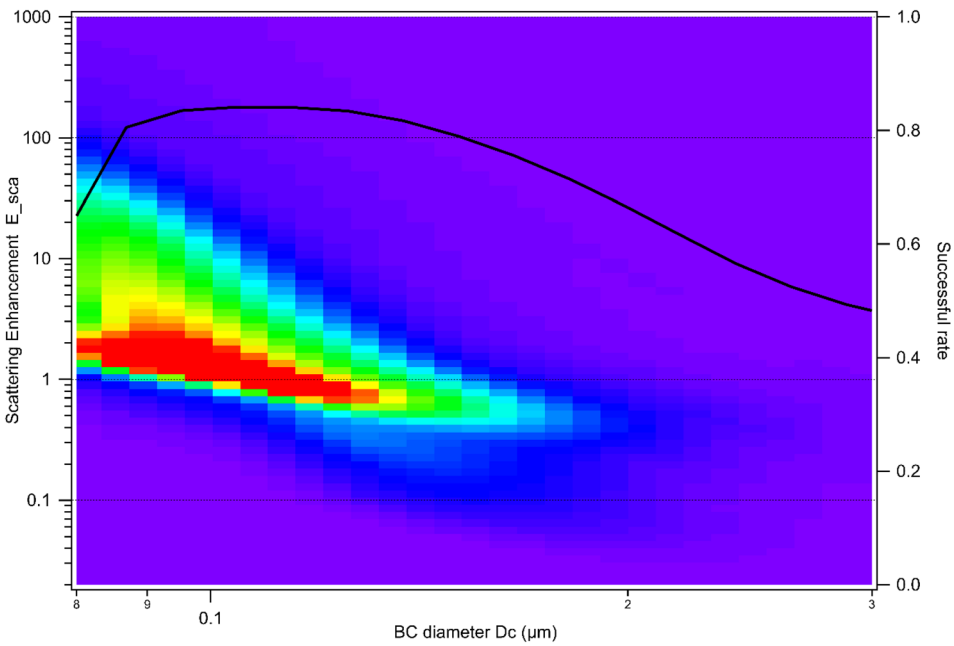

Fig. 3 BT Tower winter campaign E_{sca} 2-D histogram. Larger E_{sca} means thicker BC coating and $E_{sca} = 1$ means that BC is not coated. The colour is set to red when the particle number density is > 70% of the maximum.

 © 2025 The Author(s). Published by the Royal Society of Chemistry

Open Access Article. Published on 12 May 2025. Downloaded on 1/26/2026 6:50:53 AM.
This article is licensed under a Creative Commons Attribution 3.0 Unported Licence.

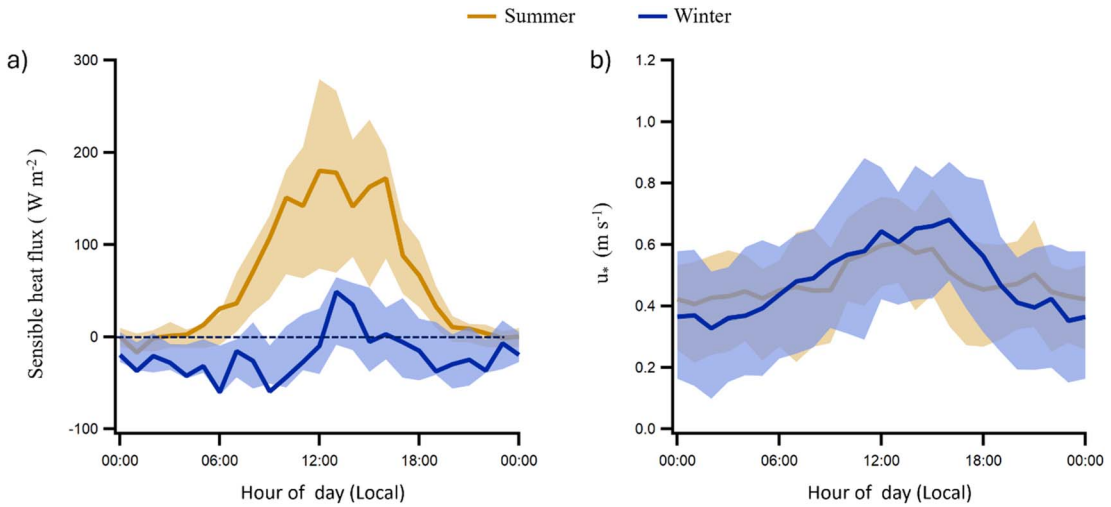

Fig. 4 Sensible heat flux (a) and friction velocity (b) in summer (yellow) and winter (blue).

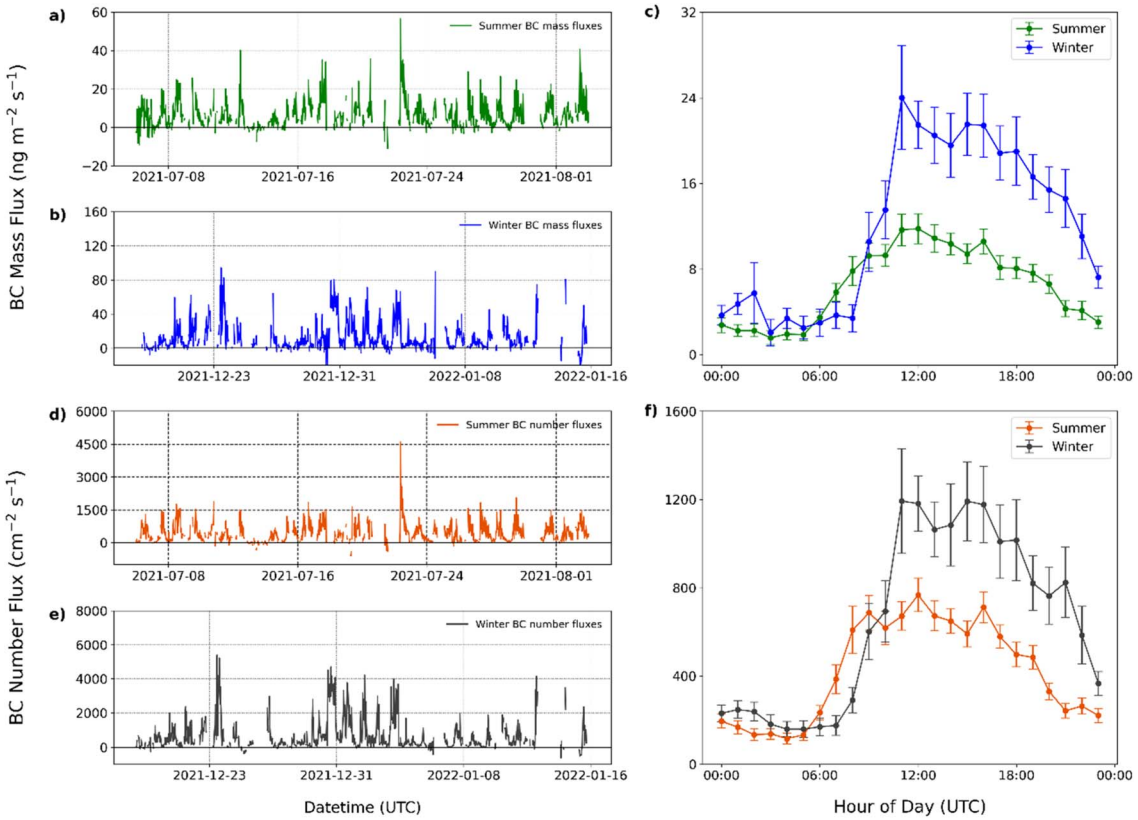

Fig. 5 BT Tower measured BC fluxes. BC mass fluxes in (a) summer and (b) winter and BC number fluxes in (d) summer and (e) winter. Diurnal profile of (c) BC mass fluxes and (f) number fluxes. Error bars in (c) and (f) represent the standard error.

a combination of reduced boundary layer mixing in the morning during winter and the impact of daylight-saving time changes.

Averaged BC mass concentrations were 0.34 μg m^{-3} in winter. This is a marked reduction from the 1.3 μg m^{-3} previously observed at an urban environment site in London in January 2012.[23] From 2019 to 2022, the introduction of the ULEZ is estimated to have reduced the $PM_{2.5}$ emissions from cars and motorcycles, vans, taxis, HGVs and buses by 37%, 15%, 57%, 27% and 60% respectively.[10] Euro 6 restrictions for on-road diesel vehicles were introduced in London from January 2014, which include the technological improvements by using improved Diesel Particulate Filters (DPFs). The change of Euro standards is estimated to have reduced on-road diesel BC

Open Access Article. Published on 12 May 2025. Downloaded on 1/26/2026 6:50:53 AM.
This article is licensed under a Creative Commons Attribution 3.0 Unported Licence.

Table 1 BC number and mass fluxes and concentration statistics in winter and summer. Calculated average of each 1 month campaign

		BC mass flux	BC number flux	BC mass concentration	BC number concentration
		ng m^{-2} s^{-1}	cm^{-2} s^{-1}	μg m^{-3}	cm^{-3}
Summer	Mean	6.826	442.5	0.2050	120.3
	Min.	−10.89	−594.5	0.0008519	10.25
	Max.	56.49	4613	0.6865	445.29
	Median	5.066	334.0	0.1701	99.40
	Standard deviation	7.093	427.2	0.1325	77.51
	Number of points	929.0	943.0	1229	1229
Winter	Mean	13.25	686.6	0.3431	146.3
	Min.	−22.35	−626.0	0.01726	12.06
	Max.	199.6	9178	4.215	1955
	Median	7.265	343.2	0.2261	95.72
	Standard deviation	17.61	950.3	0.4079	182.8
	Number of points	919.0	958.0	1327	1327

emissions by 66%.[9] The 10 year BC concentrations decreased by 70% compared to a previous study,[23] which follows the expectation of air quality policies and engine technical development in London.

3.4 Wind sector trends and spatial mapping

An indicative identification of pollution source directions can be achieved using polar plots generated with the OpenAir package in R.[44] During the summer campaign (Fig. 6a), the highest average BC emissions were associated with northeasterly winds. In contrast, during the winter (Fig. 6b), a prominent point source was evident to the southwest, characterized by a clear band with an average mass flux > 25 ng m^{-2} s^{-1}, which is also discernible in the footprint mapping plot (Fig. 7b), indicating potential emission point sources. The highlighted emission area to the northeast of the BT Tower in summer is near Euston railway station (CS1) as shown in Fig. 7a. Other studies[35,36] also reported NO_x emissions from this area, attributed to the station supporting facilities in 2017, but these were no longer significant in 2021. However, we still attribute the BC emissions at Euston station to the construction site of high-speed railway (HS2). Highlighted sources in the winter spatial map are aligned with several areas including Euston station to the northeast, high traffic roads (Marylebone Road) to the west and the point source to the southwest. NO_x fluxes hotspot areas were collocated with this HS2 construction site during both campaigns, as shown in Fig. S11.† However, the southwest point source contributes the most to BC fluxes as shown in Fig. S5a.† The dominant point source to the southwest is aligned with the operation of machinery and the use of NRMM on construction sites within the hotspot area (Fig. 7b, CS2 and CS3). CO flux hotspot areas were also collocated with these two construction sites to the southwest in both campaigns (Fig. S10†). From the NRMM usage data provided by GLA, emissions with lower than EU Stage IIIA NRMMs and

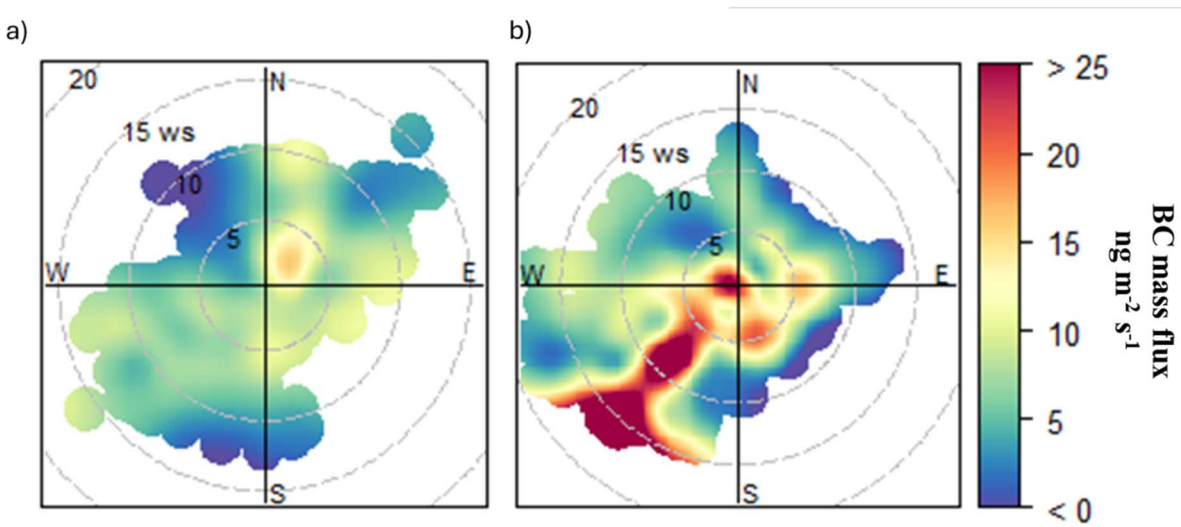

Fig. 6 BC mass flux polar plots in (a) summer and (b) winter, as a function of wind speed.

 © 2025 The Author(s). Published by the Royal Society of Chemistry

Open Access Article. Published on 12 May 2025. Downloaded on 1/26/2026 6:50:53 AM.
This article is licensed under a Creative Commons Attribution 3.0 Unported Licence.

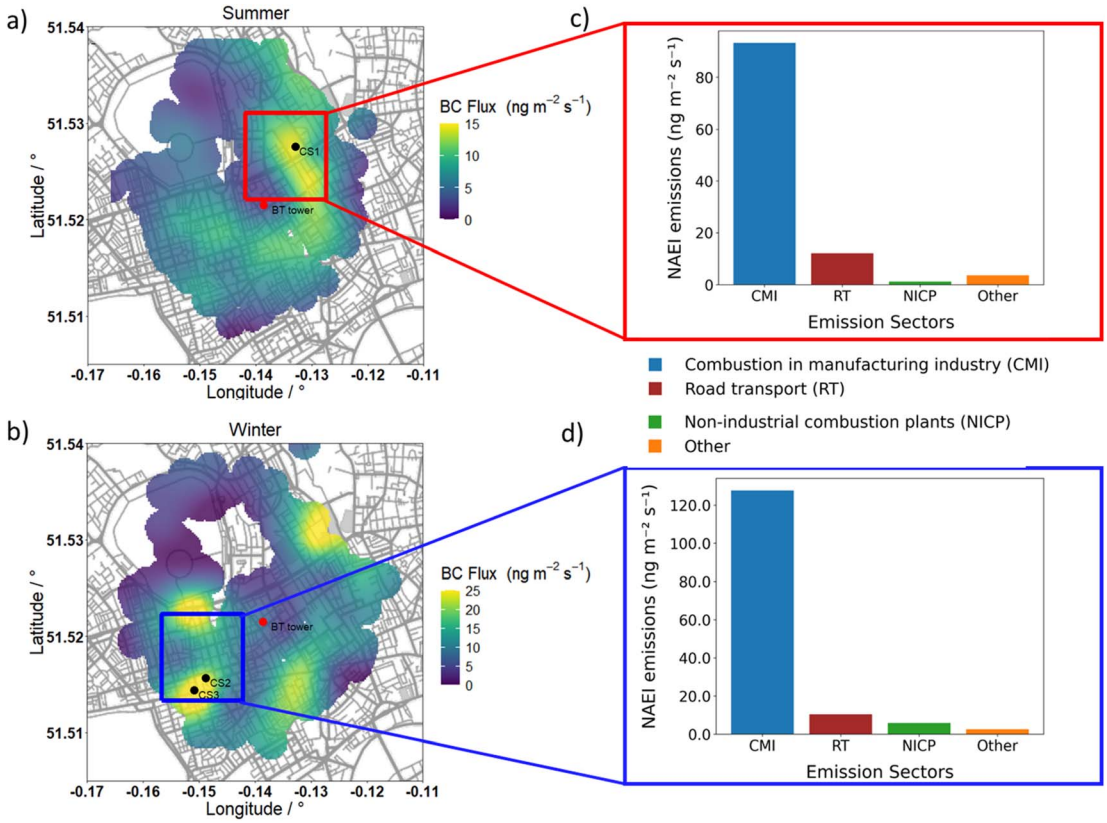

Fig. 7 Footprint spatial map in (a) summer and (b) winter with the measurement site (BT Tower) and potential construction sites (CS1, CS2, and CS3) from the construction information website[46] and Westminster City Council.[47] Together with NAEI gridded emissions in (c) northeast (red frame) and (d) southwest (blue frame).

construction machinery are still in use in the Westminster and Camden borough.[45]

3.5 Estimate of inventory emissions

The NAEI[12] is an annual and comprehensive estimate of pollutant emissions from 1970 to the present. Emission sources are categorised into 11 sectors, which are aggregated according to the United Nations Economic Commission for Europe (UNECE) Selected Nomenclature for Reporting of Air Pollutants (SNAP), while large point emission sources are reported separately.[48] For each sector, a national total emission is calculated using activity statistics data and emission rates for the pollutant emitted from the source of interest (emission factor). Spatially resolved 1 km × 1 km gridded and spatially resolved modelled estimates of NAEI emissions, including point source and area source, are provided as emission maps.[48] Two gridded areas were selected based on the major BC footprint from the NAEI spatial map, and the emissions were converted to the same unit as observed emissions (ng m^{-2} s^{-1}). The key source of BC emissions identified by the NAEI is Combustion in Manufacturing Industry (CMI), which accounts for 85% (SW) and 83% (NE) of the total BC emissions, respectively (Fig. 7c and d). Road transport (RT), non-industrial combustion plant and other sources account for 15% (SW) and 17% (NE). In the NAEI, the CMI sector is directed to manufacturing industries and construction reporting as Nomenclature for Reporting (NFR) 1.A.2, which includes 8 NFR sub-categories and is subdivided into 21 NAEI categories as shown in Tables 3–6 and 3–7 of the NAEI report.[49] In the NAEI 2021, construction NRMM (1.A.2.g.vii, hereafter referred to as NRMM) used by construction is estimated to contribute 11.4%, which is the second largest category in the CMI sector.[13] As discussed in Section 2.1, the footprint area is not expected to include manufacturing industries except construction sites as the surroundings of the BT Tower are high-density commercial areas. Therefore, the dominant BC emission source in the footprint area by observation and inventory estimation is in good agreement with respect to which construction is significant.

However, CMI emissions are estimated by the NAEI to be larger than 120 ng m^{-2} s^{-1} in winter (southwest) and >80 ng m^{-2} s^{-1} in summer (northeast), while observed BC emissions are 25 ng m^{-2} s^{-1} in winter and 15 ng m^{-2} s^{-1} in summer in the hotspot area (Fig. 7a, b and S7†). Road transport (RT) is estimated by the NAEI to be the second largest BC source in the footprint area; the NAEI emission amount matches observed emission in non-highlighted areas in Fig. 7, which are both around 10 ng m^{-2} s^{-1}.

Additionally, gridded NAEI BC emissions were also normalised to NO_x and CO to provide more comparable results. The NAEI emission ratio across all sectors of BC/NO_x (0.021 to SW,

Open Access Article. Published on 12 May 2025. Downloaded on 1/26/2026 6:50:53 AM.
This article is licensed under a Creative Commons Attribution 3.0 Unported Licence.

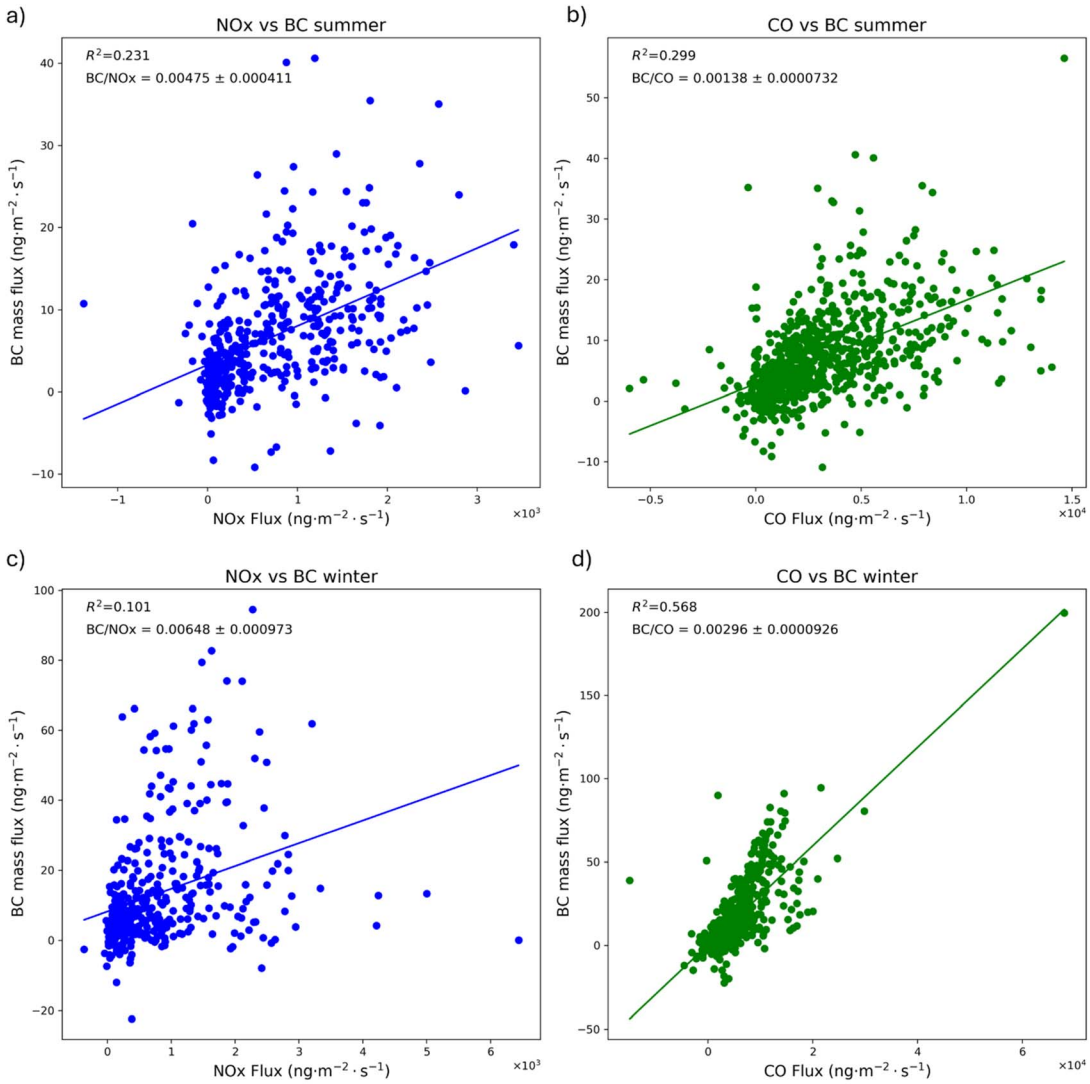

Fig. 8 NO_x flux[35] with BC mass flux in (a) summer and (c) winter and CO with BC mass flux in (b) summer and (d) winter. Uncertainties in the BC/NO_x and BC/CO ratios are represented by the standard deviation.

0.018 to NE) is around 3.2 and 3.5 times larger than the observed ratios in winter and summer (Fig. 8a and c), while BC/CO (0.035 to SW, 0.048 to NE) ratios were 32.4 and 12.5 times larger than observations in winter and summer (Fig. 8b and d). Comparing the total emissions and ratios between NAEI and observations, the overestimate in the NAEI may mainly come from CMI sectors rather than RT.

Better agreement is found after removing the CMI sector, with the NAEI BC being 23 ng m^{-2} s^{-1} (SW) and 19 ng m^{-2} s^{-1} (NE). BC/NO_x (0.012 to SW, 0.010 to NE) ratios were 1.9 and 2.1 times larger than observations, while BC/CO (0.006833 to SW and 0.013 to NE) ratios were 2.4 and 10 times larger than observations. CMI emissions are calculated using fuel consumption data from UK statistics (DUKES) and default emission factors from the European Environment Agency (EEA) using the NAEI Tier 3 methodology, which includes complex model approaches to provide accuracy estimation.[49] Construction NRMM emission estimation in NAEI uses the EEA default BC emission factor, which represents global average performance rather than accurate UK circumstances. Furthermore, construction sites are not identified as BC point sources in the NAEI even if they make a significant contribution. Even off-road emissions are mapped using revised employment statistics,[48] which removes some cases in the urban area, and NRMM emissions are still overestimated in NAEI 2021. However, the highly episodic and spatial granularity of construction sites would also make the estimation difficult.

3.6 Comparisons with other fluxes

Other pollutants may co-emit with BC from the sources. NO_x and CO were selected for comparison with BC because of their significant contributions to construction and road transport.[30,50] The orthogonal distance regression linear correlations of BC, NO_x and CO are shown in Fig. 8. Low correlations between BC and NO_x in summer ($R^2 = 0.23$) and winter ($R^2 = 0.10$) are likely due to the prominence of gas combustion in boilers, which now dominates NO_x emissions in central

 © 2025 The Author(s). Published by the Royal Society of Chemistry

Open Access Article. Published on 12 May 2025. Downloaded on 1/26/2026 6:50:53 AM.
This article is licensed under a Creative Commons Attribution 3.0 Unported Licence.

London.[35] This combustion is much cleaner and has much lower BC emissions compared to other sources like diesel internal combustion engines.

A stronger correlation between BC and CO in winter ($R^2 = 0.57$) and summer ($R^2 = 0.30$) suggests that these pollutants are co-emitted in central London. Road transport and other mobile machinery are estimated by the NAEI to be the biggest contributors to CO emissions around the BT Tower. With the introduction of Euro 6 diesel engines and the ULEZ policy, as well as the proliferation of electric vehicles, BC emissions from road transport are less obvious. Therefore, the BC and CO correlation gives confidence that construction NRMM is the main source of BC.

Winter BC mass fluxes were observed to be 48% larger than those in summer. Similarly, winter BC/NO_x and BC/CO ratios were 27% and 53% higher, respectively, compared to summer. These differences may be attributed to reduced industrial and traffic emissions during the COVID-19 pandemic affecting the summer period, but equally also to additional winter sources such as heating and vehicle cold starts. The representative construction activities around the BT Tower rose by 22% in the winter campaign period compared to the summer.[45] The representative traffic flow in winter was 3.7% smaller than that in summer.[35] The rise in BC/NO_x ratios aligns with the 22% increase in construction activity. The rise in BC/CO is likely influenced by cold starts in winter, contributing to the 53% increase. Consequently, differences in BC emissions between winter and summer appear to be driven by a combination of changes in construction and traffic activities.

The UK follows the EEA regulation system for non-road machinery emission controls, which covers major pollutants including NO_x, CO, PM and hydrocarbons.[51] The EEA emission standards include BC/$PM_{2.5}$ emission ratios categorized by engine types and power ratings. To better understand construction NRMM contributions to BC emissions, BC/CO and BC/NO_x ratios were calculated from non-road machinery EEA regulations (Table 2). Given that NO_x and BC are not co-emitted from gas combustion to the northeast of BT Tower, we selected the southwest BC/NO_x, ratio which is more related ($R^2 = 0.28$ in summer, $R^2 = 0.27$ in winter) to BC (Fig. S8a and b†) to compare with the EEA NRMM standard. Comparing the ratios measured from the BT Tower as shown in Fig. 8, we find good agreement for EU Stage IIIB, IV (no DPF) and V, which match the requirements of ULEZ NRMM standards.[52]

However, in the footprint area the policy for NRMM emission control lags behind those for the road vehicle standard level (*e.g.* ULEZ), and it is likely the reason why construction BC emissions stand out. The GLA pledged to develop nearly 60 000 jobs and 50 000 housing units in London after becoming one of the largest landowners.[53] Large generators and NRMM operating at construction sites significantly contribute to air pollution, accounting for 34% of PM_{10} and 14% of $PM_{2.5}$, which are the largest and second-largest sources in London, respectively.[50,54] NRMM and generator registration data provided by the GLA for the Westminster and Camden boroughs reveal evidence of high-power-rate machinery usage (greater than 130 kW h) around the BT Tower during both campaign periods. Although time series on machinery usage for specific sites cannot be examined, the evidence above is substantial enough to raise concerns about BC emissions from the construction industry in central London. Similar concerns regarding gas and particulate pollutants from NRMM have been raised.[50] The GLA also has future plans in London for NRMM emission control in the ULEZ to meet Stage IV by 2025 and Stage V by 2030, as well as zero emissions by 2040.[52] Consequently, it is imperative to continuously emphasise the importance of this sector for BC emissions and to address the uncertainties in inventory estimates for construction activities in the coming years. National strategies and policies, such as the industrial decarbonisation strategy,[55] will require further infrastructure development, potentially increasing emissions from NRMM sources if not effectively regulated.

3.7 Comparisons with other cities

Previous studies conducted observations of BC fluxes from a tower (102 m) in Beijing[17] during the winter of 2016 (mean: 5.49 ng m^{-2} s^{-1}) and the summer of 2017 (mean: 6.10 ng m^{-2} s^{-1}), and in Delhi[19] from a 35 m tower during November 2018 (mean: 25.8 ng m^{-2} s^{-1}). All fluxes are whole campaign averages. In the studies of these three cities, emission inventories overestimate BC emissions in urban areas. BC fluxes in London from this study were similar to fluxes in Beijing in summer and twice as high as in Beijing in winter, while 3.5 (summer) and 2.0 (winter) times lower than in Delhi. During observations in the 3 cities, London had introduced Euro 6 for on-road vehicles, while Beijing was on China 5 (Euro 5) controls, while Delhi was on the Bharat Stage IV (Euro 4) standard. Moreover, Beijing and Delhi diesel powered vehicles were only allowed during nighttime and Beijing's vehicle fleet was ahead in terms of electrification. Thus, direct comparisons between urban flux measurement datasets need to be made with caution due to differences in local emission controls,[56,57] as well as site characteristics.[58] Some measurements might be taken in more intensely urban areas than others, while meteorological conditions would also be different.[59,60] To eliminate this latter effect, Beijing BC fluxes are normalised by NO_x and CO[17] for comparison to evaluate traffic and construction BC emissions. Delhi BC[19] NO_x and CO fluxes[61] are retrieved for the corresponding comparisons. Since Bharat Stage IV (Euro 4) standards were used as on-road vehicle emissions, BC emissions were thought to have been dominated by road traffic in Delhi (Table 3).

The primary source for BC emissions in Beijing was attributable to gasoline traffic contributions accounting for 92% of the total flux.[17] We are not aware of any major construction sites operating inside the footprint area during the Beijing measurements. For traffic control, Beijing has banned the entry of diesel vehicles during the daytime, leading to BC emissions lower than in London even under the China 5 (Euro 5) standard. However, the BC concentrations in Beijing are much higher than in London, which may be due to transportation from the wider north plain or rural area or limited diffusion conditions due to the shallow boundary layer. This increases the concerns about both construction contribution and the impact of traffic

Open Access Article. Published on 12 May 2025. Downloaded on 1/26/2026 6:50:53 AM.
This article is licensed under a Creative Commons Attribution 3.0 Unported Licence.

Table 2 Non-road machinery (1A2.gvii) emission standard with EU Stage I to V BC/CO and BC/NO_x ratios,[51] compared with BT Tower observations. From stage IIIB, diesel particulate filters (DPFs) are applied to the engine. The "EU Stage" column indicates engine categories (EU Stage I to V), with sub-categories denoted by letters A to R for EU Stage I to IV and by codes c-1 to c-7 for non-road engines (NREs) at EU Stage V, reflecting different power rate bands. Generator is shown as a distinct sub-category in EU Stage V. Engine power rate (P) bands are shown in the column "Engine size" with units of kW h. BC/CO and BC/NO_x columns represent the ratios of EU standard categories and observations. Front slash ("/") denotes no data. Observed BC/CO ratios correspond to the total footprint area, while observed BC/NO_x ratios are reported separately for the total footprint and southwest areas. Observed ratios include mean values and standard deviation from each measurement campaign

Non-road diesel			
EU stage	Engine size	BC/CO	BC/NO_x
Stage I power rate (P, kW h)			
A	$130 \leq P < 560$	0.0756	0.0411
B	$75 \leq P < 130$	0.112	0.0609
C	$37 \leq P < 75$	0.105	0.739
Stage II			
D	$18 \leq P < 37$	0.116	0.080
E	$130 \leq P < 560$	0.0400	0.233
F	$75 \leq P < 130$	0.0480	0.0400
G	$37 \leq P < 75$	0.0640	0.0457
Stage IIIA			
H	$130 \leq P < 560$	0.0400	—
I	$75 \leq P < 130$	0.0480	—
J	$37 \leq P < 75$	0.0640	—
K	$19 \leq P < 37$	0.0873	—
Stage IIIB, no DPF			
L	$130 \leq P < 560$	0.00500	0.00875
M	$75 \leq P < 130$	0.00350	0.00530
N	$56 \leq P < 75$	0.00350	0.00530
P	$37 \leq P < 56$	0.00350	—
Stage IIIB, DPF			
L	$130 \leq P < 560$	0.00107	0.001875
M	$75 \leq P < 130$	0.000750	0.00114
N	$56 \leq P < 75$	0.000750	0.00114
P	$37 \leq P < 56$	0.000750	—
Stage IV, no DPF			
Q	$130 \leq P < 560$	0.00500	0.0438
R	$56 \leq P < 130$	0.00350	0.0438
Stage IV, DPF			
Q	$130 \leq P < 560$	0.00107	0.00938
R	$56 \leq P < 130$	0.000750	0.00938
Stage V			
NRE-v/c-7	$P > 560$	0.00193	0.00193
NRE-v/c-6	$130 \leq P \leq 560$	0.000429	0.00563
NRE-v/c-5	$56 \leq P < 130$	0.000450	0.00563
NRE-v/c-4	$37 \leq P < 56$	0.000450	—
NRE-v/c-3	$19 \leq P < 37$	0.000450	—
NRE-v/c-2	$8 \leq P < 19$	0.00909	—
NRE-v/c-1	$P < 8$	0.00750	—
Generators	$P > 560$	0.00784	0.00150
Observations			
Winter		0.00296 ± 0.0000926 (total)	0.00648 ± 0.000973 (total) 0.0168 ± 0.00181 (SW)
Summer		0.00138 ± 0.0000732 (total)	0.00475 ± 0.000471 (total) 0.00536 ± 0.000609 (SW)

 © 2025 The Author(s). Published by the Royal Society of Chemistry

Open Access Article. Published on 12 May 2025. Downloaded on 1/26/2026 6:50:53 AM.
This article is licensed under a Creative Commons Attribution 3.0 Unported Licence.

Table 3 Observations of averaged BC number and mass fluxes. BC/NO_x and BC/CO ratios in Beijing, London and Delhi (with the standard deviation)

Seasons	Location	BC number flux mean (cm^{-2} s^{-1})	BC mass flux mean (ng m^{-2} s^{-1})	BC/NO_x	BC/CO
Summer	Beijing	334.37	6.10	0.0052	0.0011
	London	442.50	6.83	0.0048 ± 0.00047	0.0014 ± 0.000073
Winter	Beijing	261.25	5.49	0.0058	0.0007
	London	686.60	13.3	0.0065 ± 0.00097	0.0030 ± 0.000093
Post-monsoon	Delhi	850.00	25.8	0.0011 ± 0.00089	0.00036 ± 0.00065

control policies on BC emissions in the London ULEZ area. Normalised summer BC emissions have no significant difference in Beijing and London, which is due to low human activities (especially less construction site operation) during the COVID pandemic in London. The London winter BC/CO flux ratio was four times larger than in Beijing, indicating additional non-gasoline BC sources in London. Cold starts in Beijing leading to high CO emissions could also be the potential reason for low BC/CO ratios. The London BC/NO_x flux ratio was 4.4 times (summer) and 5.9 times (winter) larger than in Delhi. The potential reason could be nighttime NO storage leading to high NO_x emissions in the daytime when the nighttime boundary layer collapse.[62] The Delhi BC/CO ratio has large uncertainty due to a lack of matched data points (53 matched data points). However, bearing in mind the uncertainties in the correlations, the comparable agreement of normalized BC emissions between Beijing and London nevertheless enhances confidence in quantifying urban BC emissions using EC fluxes.

4 Conclusion

In this study, BC emissions in central London during two different seasons were quantified using the eddy covariance technique. We found that BC mass and number fluxes in winter (13.3 ng m^{-2} s^{-1} and 687 cm^{-2} s^{-1}) were approximately twice as high as those in summer (6.83 ng m^{-2} s^{-1} and 443 cm^{-2} s^{-1}) due to increased construction sites resulting from increasing human activities after COVID. Thick BC coatings were absent compared to earlier measurements in 2012, indicating traffic associated BC emissions are dominant in central London rather than biomass burning. Footprint analysis highlighted that BC emission sources were associated with construction sites. Comparisons with the spatially resolved NAEI revealed that the construction sector is the dominant source of BC emissions in the footprint area. Quantitatively, the measured emissions agreed well with the NAEI for most sources, but construction was overestimated in the NAEI by a factor of 5–6 compared to the observations due to less representative emission factors and spatial data use. However, it is recognised that quantitatively accounting for source within inventories is extremely challenging due to its spatial granularity and highly episodic nature. Comparisons of BC/NO_x and BC/CO ratios with EEA emission standards raise additional concerns for large machinery used in the construction industry. It is encouraged to increase the spatial coverage of BC measurements for better identifying hotspots in urban emission studies in the future.

BC concentrations in London have significantly decreased since the introduction of the ULEZ and the use of more efficient diesel particulate filters in Euro 6 road diesel vehicles. However, to meet the WHO guidelines for urban air quality and address human health concerns, air quality in London can be further improved by introducing tightened regulation for NRMM. The conclusions from this study also highlight concerns about NRMM in other countries with high construction demands.

Data availability

The EddyPro software to generate fluxes and 1-D footprints can be freely downloaded at **https://www.licor.com/support/EddyPro/software.html**. The R package OpenAir used to generate polar plots and spatial flux footprints on the map can be freely accessed at **https://github.com/openair-project/openair**. NAEI data for Fig. 7 have been taken from the National Atmospheric Emission Inventory website (**https://naei.energysecurity.gov.uk/**). The ERA5 boundary layer height data can be accessed at **https://cds.climate.copernicus.eu/cdsapp#!/home** or **https://cds.climate.copernicus.eu/**. The construction operation data used in this study were provided by the GLA from freedom of information at (**https://www.london.gov.uk/programmes-and-strategies/environment-and-climate-change/pollution-and-air-quality/nrmm**). The processed BC fluxes data are available on the Centre for Environmental Data Analysis Archive (**https://catalogue.ceda.ac.uk/uuid/ab605b618884401c91afd0274c92144e/**).

Author contributions

ZC made BC measurements, calculated the fluxes, performed footprint modelling and analysed the data. ZC wrote the paper and produced the figures. JA, MF, EN, and JC provided support with the measurements from sites. JA, DH, DL, and RJ provided support with the SP2 data processing. DH provided training on SP2 toolkits software. JA, EN, BL, CH, and RJ provided support with the flux calculations. BL and CH provided meteorological data and explanation. WD provided support with footprint modelling and the codes. CH provided CO flux data. SC provided NO_x flux data and traffic activity data. All authors read and commented on the paper.

Open Access Article. Published on 12 May 2025. Downloaded on 1/26/2026 6:50:53 AM.
This article is licensed under a Creative Commons Attribution 3.0 Unported Licence.

Conflicts of interest

The authors declare no conflict of interest.

Acknowledgements

This work was funded by UKRI through the OSCA project (grant ref. NE/T001984/1 and NE/T001798/2), part of the NERC Clean Air Strategic Priorities Fund. The BT Tower Atmospheric Observatory is supported by NERC through the UKCEH National Capability for UK Challenges Programme – NE/Y006208/1. The authors thank Neil Mullinger (UK Centre for Ecology and Hydrology) for instrument and sample line maintenance and BT for granting access to the BT Tower for research. The authors also thank Carl Desouza and David Green (Imperial College London) for guidance in locating construction operation data.

References

1 WHO, *World Health Organisation Ambient (Outdoor) Air Pollution*, https://www.who.int/news-room/fact-sheets/detail/ambient-(outdoor)-air-quality-and-health.

2 T. C. Bond, S. J. Doherty, D. W. Fahey, P. M. Forster, T. Berntsen, B. J. Deangelo, M. G. Flanner, S. Ghan, B. Kärcher, D. Koch, S. Kinne, Y. Kondo, P. K. Quinn, M. C. Sarofim, M. G. Schultz, M. Schulz, C. Venkataraman, H. Zhang, S. Zhang, N. Bellouin, S. K. Guttikunda, P. K. Hopke, M. Z. Jacobson, J. W. Kaiser, Z. Klimont, U. Lohmann, J. P. Schwarz, D. Shindell, T. Storelvmo, S. G. Warren and C. S. Zender, Bounding the role of black carbon in the climate system: a scientific assessment, *J. Geophys. Res.: Atmos.*, 2013, **118**, 5380–5552.

3 E. J. Highwood and R. P. Kinnersley, When smoke gets in our eyes: the multiple impacts of atmospheric black carbon on climate, air quality and health, *Environ. Int.*, 2006, **32**, 560–566.

4 J. L. Nichols, E. O. Owens, S. J. Dutton and T. J. Luben, Systematic review of the effects of black carbon on cardiovascular disease among individuals with pre-existing disease, *Int. J. Public Health*, 2013, **58**, 707–724.

5 W. J. Gauderman, E. Avol, F. Gilliland, H. Vora, D. Thomas, K. Berhane, R. McConnell, N. Kuenzli, F. Lurmann, E. Rappaport, H. Margolis, D. Bates and J. Peters, The Effect of Air Pollution on Lung Development from 10 to 18 Years of Age, *N. Engl. J. Med.*, 2004, **351**, 1057–1067.

6 WHO, *WHO Global Air Quality Guidelines: Particulate Matter ($PM_{2.5}$ and PM_{10}), Ozone, Nitrogen Dioxide, Sulfur Dioxide and Carbon Monoxide*, 2021.

7 United Nations Environment Programme and WMO, *Integrated Assessment of Black Carbon and Tropospheric Ozone*, 2011.

8 GLA, *Expanded Ultra Low Emission Zone – First Month Report|London City Hall*, https://www.london.gov.uk/programmes-and-strategies/environment-and-climate-change/environment-publications/expanded-ultra-low-emission-zone-first-month-report.

9 L. Ntziachristos and Z. Samaras, *EMEP/EEA Air Pollutant Emission Inventory Guidebook 2023*, 2023.

10 GLA, *Inner London Ultra Low Emission Zone Expansion One Year Report|London City Hall*, https://www.london.gov.uk/programmes-strategies/environment-and-climate-change/environment-and-climate-change-publications/inner-london-ultra-low-emission-zone-expansion-one-year-report#background-165719-title.

11 J. D. Lee, C. Helfter, R. M. Purvis, S. D. Beevers, D. C. Carslaw, A. C. Lewis, S. J. Møller, A. Tremper, A. Vaughan and E. G. Nemitz, Measurement of NO_x Fluxes from a Tall Tower in Central London, UK and Comparison with Emissions Inventories, *Environ. Sci. Technol.*, 2015, **49**, 1025–1034.

12 NAEI, *NAEI, UK National Atmospheric Emissions Inventory*, NAEI, UK, https://naei.beis.gov.uk/.

13 NAEI, *UK Spatial Emissions Methodology A Report of the National Atmospheric Emission Inventory 2020*, 2022.

14 U. Paliwal, M. Sharma and J. F. Burkhart, Monthly and spatially resolved black carbon emission inventory of India: uncertainty analysis, *Atmos. Chem. Phys.*, 2016, **16**, 12457–12476.

15 H. Simon, D. T. Allen and A. E. Wittig, Fine Particulate Matter Emissions Inventories: Comparisons of Emissions Estimates with Observations from Recent Field Programs, *J. Air Waste Manage. Assoc.*, 2008, **58**, 320–343.

16 E. Nemitz, J. L. Jimenez, J. A. Huffman, I. M. Ulbrich, M. R. Canagaratna, D. R. Worsnop and A. B. Guenther, An Eddy-Covariance System for the Measurement of Surface/Atmosphere Exchange Fluxes of Submicron Aerosol Chemical Species—First Application Above an Urban Area, *Aerosol Sci. Technol.*, 2008, **42**, 636–657.

17 R. Joshi, D. Liu, E. Nemitz, B. Langford, N. Mullinger, F. Squires, J. Lee, Y. Wu, X. Pan, P. Fu, S. Kotthaus, S. Grimmond, Q. Zhang, R. Wu, O. Wild, M. Flynn, H. Coe and J. Allan, Direct measurements of black carbon fluxes in central Beijing using the eddy covariance method, *Atmos. Chem. Phys.*, 2021, **21**, 147–162.

18 E. W. Emerson, J. M. Katich, J. P. Schwarz, G. R. McMeeking and D. K. Farmer, Direct Measurements of Dry and Wet Deposition of Black Carbon Over a Grassland, *J. Geophys. Res.: Atmos.*, 2018, **123**(12), 212–277, 290.

19 R. Joshi, *Black carbon flux measurements in megacities using the eddy covariance method*, 2021.

20 S. E. Lane, J. F. Barlow and C. R. Wood, An assessment of a three-beam Doppler lidar wind profiling method for use in urban areas, *J. Wind. Eng. Ind. Aerodyn.*, 2013, **119**, 53–59.

21 R. S. Gao, J. P. Schwarz, K. K. Kelly, D. W. Fahey, L. A. Watts, T. L. Thompson, J. R. Spackman, J. G. Slowik, E. S. Cross, J. H. Han, P. Davidovits, T. B. Onasch and D. R. Worsnop, A Novel Method for Estimating Light-Scattering Properties of Soot Aerosols Using a Modified Single-Particle Soot Photometer, *Aerosol Sci. Technol.*, 2007, **41**, 125–135.

22 H. A. Michelsen, C. Schulz, G. J. Smallwood and S. Will, Laser-induced incandescence: Particulate diagnostics for combustion, atmospheric, and industrial applications, *Prog. Energy Combust. Sci.*, 2015, **51**, 2–48.

 © 2025 The Author(s). Published by the Royal Society of Chemistry

Open Access Article. Published on 12 May 2025. Downloaded on 1/26/2026 6:50:53 AM.
This article is licensed under a Creative Commons Attribution 3.0 Unported Licence.

23 D. Liu, J. D. Allan, D. E. Young, H. Coe, D. Beddows, Z. L. Fleming, M. J. Flynn, M. W. Gallagher, R. M. Harrison, J. Lee, A. S. H. Prevot, J. W. Taylor, J. Yin, P. I. Williams and P. Zotter, Size distribution, mixing state and source apportionment of black carbon aerosol in London during wintertime, *Atmos. Chem. Phys.*, 2014, **14**, 10061–10084.

24 M. Laborde, M. Schnaiter, C. Linke, H. Saathoff, K. H. Naumann, O. Möhler, S. Berlenz, U. Wagner, J. W. Taylor, D. Liu, M. Flynn, J. D. Allan, H. Coe, K. Heimerl, F. Dahlkötter, B. Weinzierl, A. G. Wollny, M. Zanatta, J. Cozic, P. Laj, R. Hitzenberger, J. P. Schwarz and M. Gysel, Single particle soot photometer intercomparison at the AIDA chamber, *Atmos. Meas. Tech.*, 2012, **5**, 3077–3097.

25 D. Liu, J. Whitehead, M. R. Alfarra, E. Reyes-Villegas, D. V. Spracklen, C. L. Reddington, S. Kong, P. I. Williams, Y.-C. Ting, S. Haslett, J. W. Taylor, M. J. Flynn, W. T. Morgan, G. McFiggans, H. Coe and J. D. Allan, Black-carbon absorption enhancement in the atmosphere determined by particle mixing state, *Nat. Geosci.*, 2017, **10**, 184–188.

26 J. W. Taylor, J. D. Allan, D. Liu, M. Flynn, R. Weber, X. Zhang, B. L. Lefer, N. Grossberg, J. Flynn and H. Coe, Assessment of the sensitivity of core/shell parameters derived using the single-particle soot photometer to density and refractive index, *Atmos. Meas. Tech.*, 2015, **8**, 1701–1718.

27 N. Moteki, Y. Kondo and S.-i. Nakamura, Method to measure refractive indices of small nonspherical particles: application to black carbon particles, *J. Aerosol Sci.*, 2010, **41**, 513–521.

28 D. Liu, R. Joshi, J. Wang, C. Yu, J. D. Allan, H. Coe, M. J. Flynn, C. Xie, J. Lee, F. Squires, S. Kotthaus, S. Grimmond, X. Ge, Y. Sun and P. Fu, Contrasting physical properties of black carbon in urban Beijing between winter and summer, *Atmos. Chem. Phys.*, 2019, **19**, 6749–6769.

29 T. Foken, M. Aubinet and R. Leuning, in *Eddy Covariance: A Practical Guide to Measurement and Data Analysis*, ed. M. Aubinet, T. Vesala and D. Papale, Springer Netherlands, Dordrecht, 2012, pp. 1–19, DOI: 10.1007/978-94-007-2351-1_1.

30 C. Helfter, A. H. Tremper, C. H. Halios, S. Kotthaus, A. Bjorkegren, C. S. B. Grimmond, J. F. Barlow and E. Nemitz, Spatial and temporal variability of urban fluxes of methane, carbon monoxide and carbon dioxide above London, UK, *Atmos. Chem. Phys.*, 2016, **16**, 10543–10557.

31 B. Langford, P. K. Misztal, E. Nemitz, B. Davison, C. Helfter, T. A. M. Pugh, A. R. MacKenzie, S. F. Lim and C. N. Hewitt, Fluxes and concentrations of volatile organic compounds from a South-East Asian tropical rainforest, *Atmos. Chem. Phys.*, 2010, **10**, 8391–8412.

32 G. Burba, *Eddy Covariance Method for Scientific, Regulatory, and Commercial Applications*, 2022.

33 D. Vickers and L. Mahrt, Quality Control and Flux Sampling Problems for Tower and Aircraft Data, *J. Atmos. Ocean. Technol.*, 1997, **14**, 512–526.

34 T. Foken, in *Micrometeorology*, ed. T. Foken, Springer Berlin Heidelberg, Berlin, Heidelberg, 2017, pp. 143–205, DOI: 10.1007/978-3-642-25440-6_4.

35 S. J. Cliff, W. Drysdale, J. D. Lee, C. Helfter, E. Nemitz, S. Metzger and J. F. Barlow, Pandemic restrictions in 2020 highlight the significance of non-road NO_x sources in central London, *Atmos. Chem. Phys.*, 2023, **23**, 2315–2330.

36 W. S. Drysdale, A. R. Vaughan, F. A. Squires, S. J. Cliff, S. Metzger, D. Durden, N. Pingintha-Durden, C. Helfter, E. Nemitz, C. S. B. Grimmond, J. Barlow, S. Beevers, G. Stewart, D. Dajnak, R. M. Purvis and J. D. Lee, Eddy covariance measurements highlight sources of nitrogen oxide emissions missing from inventories for central London, *Atmos. Chem. Phys.*, 2022, **22**, 9413–9433.

37 J. M. Wilczak, S. P. Oncley and S. A. Stage, Sonic Anemometer Tilt Correction Algorithms, *Bound.-Layer Meteorol.*, 2001, **99**, 127–150.

38 J. H. C. Gash and A. D. Culf, Applying a linear detrend to eddy correlation data in realtime, *Bound.-Layer Meteorol.*, 1996, **79**, 301–306.

39 M. Mauder and T. Foken, Impact of post-field data processing on eddy covariance flux estimates and energy balance closure, *Meteorol. Z.*, 2006, **15**, 597–609.

40 J. C. Kaimal and J. J. Finnigan, *Atmospheric Boundary Layer Flows: Their Structure and Measurement*, Oxford University Press, 1994.

41 S. P. Oncley, C. A. Friehe, J. C. Larue, J. A. Businger, E. C. Itsweire and S. S. Chang, Surface-layer fluxes, profiles, and turbulence measurements over uniform terrain under near-neutral conditions, *J. Atmos. Sci.*, 1996, **53**, 1029–1044.

42 R. L. Desjardins, J. I. Macpherson, P. H. Schuepp and F. Karanja, in *Boundary Layer Studies and Applications: A Special Issue of Boundary-Layer Meteorology in Honor of Dr Hans A. Panofsky (1917–1988)*, ed. R. E. Munn, Springer Netherlands, Dordrecht, 1989, pp. 55–69, DOI: 10.1007/978-94-009-0975-5_5.

43 N. Kljun, P. Calanca, M. W. Rotach and H. P. Schmid, A Simple Parameterisation for Flux Footprint Predictions, *Bound.-Layer Meteorol.*, 2004, **112**, 503–523.

44 D. C. Carslaw and K. Ropkins, Openair — an R package for air quality data analysis, *Environ. Model. Softw.*, 2012, **27–28**, 52–61.

45 GLA, *Greater London Authority Construction Sites*, 2023.

46 Considerate Constructors Scheme, *Construction Map*, https://www.constructionmap.info/, accessed 2021/12/17.

47 WCC, Westminster City Council, https://www.westminster.gov.uk/, accessed 2024/05/20, 2024.

48 I. Tsagatakis, J. Richardson, C. Evangelides, M. Pizzolato, B. Richmond, S.-M. Hows, B. Pearson, N. Passant, M. Pommier and A. Otto, *UK Spatial Emissions Methodology: A Report of the National Atmospheric Emission Inventory 2021*, 2023.

49 M. Elliott, D. Ingledew, B. Richmond, S. Del Vento, S. Gorji, N. Hamilton, E. Karagianni, A. Kelsall, Y. Pang, N. Passant, B. Pearson, J. Richardson, R. Stewart, G. Thistlethwaite, I. Tsagatakis, D. Wakeling, J. Wiltshire, J. Wong,

Open Access Article. Published on 12 May 2025. Downloaded on 1/26/2026 6:50:53 AM.
This article is licensed under a Creative Commons Attribution 3.0 Unported Licence.

M. Hobson, A. Carswell, U. Dragosits and S. Anthony, *UK Informative Inventory Report (1990 to 2022)*, 2024.

50 C. D. Desouza, D. J. Marsh, S. D. Beevers, N. Molden and D. C. Green, Real-world emissions from non-road mobile machinery in London, *Atmos. Environ.*, 2020, **223**, 117301.

51 M. Winther, C. Dore, U. Lambrecht, J. Norris, Z. Samaras and K.-H. Zierock, *EMEP/EEA Air Pollutant Emission Inventory Guidebook 2023*, 2023, **https://www.eea.europa.eu/en**.

52 GLA, *Non-Road Mobile Machinery (NRMM) Practical Guide v.6*, 2024, **https://www.london.gov.uk/sites/default/files/2024-05/NRMM-Practical-Guide-Accessible-May2024.pdf**.

53 GLA, *Development sites map|London City Hall*, **https://www.london.gov.uk/programmes-strategies/housing-and-land/land-and-development/development-sites-map**.

54 C. D. Desouza, D. J. Marsh, S. D. Beevers, N. Molden and D. C. Green, A spatial and fleet disaggregated approach to calculating the NOX emissions inventory for non-road mobile machinery in London, *Atmos. Environ.: X*, 2021, **12**, 100125.

55 UK Government, *Industrial Decarbonisation Strategy*, 2021.

56 Y. Wu, S. Zhang, J. Hao, H. Liu, X. Wu, J. Hu, M. P. Walsh, T. J. Wallington, K. M. Zhang and S. Stevanovic, On-road vehicle emissions and their control in China: A review and outlook, *Sci. Total Environ.*, 2017, **574**, 332–349.

57 S. Chowdhury, S. Dey, S. N. Tripathi, G. Beig, A. K. Mishra and S. Sharma, "Traffic intervention" policy fails to mitigate air pollution in megacity Delhi, *Environ. Sci. Policy*, 2017, **74**, 8–13.

58 G. Nicolini, G. Antoniella, F. Carotenuto, A. Christen, P. Ciais, C. Feigenwinter, B. Gioli, S. Stagakis, E. Velasco, R. Vogt, H. C. Ward, J. Barlow, N. Chrysoulakis, P. Duce, M. Graus, C. Helfter, B. Heusinkveld, L. Järvi, T. Karl, S. Marras, V. Masson, B. Matthews, F. Meier, E. Nemitz, S. Sabbatini, D. Scherer, H. Schume, C. Sirca, G.-J. Steeneveld, C. Vagnoli, Y. Wang, A. Zaldei, B. Zheng and D. Papale, Direct observations of CO2 emission reductions due to COVID-19 lockdown across European urban districts, *Sci. Total Environ.*, 2022, **830**, 154662.

59 Y. Wu, R. Zhang, P. Tian, J. Tao, S. C. Hsu, P. Yan, Q. Wang, J. Cao, X. Zhang and X. Xia, Effect of ambient humidity on the light absorption amplification of black carbon in Beijing during January 2013, *Atmos. Environ.*, 2016, **124**, 217–223.

60 V. Ramanathan, C. Chung, D. Kim, T. Bettge, L. Buja, J. T. Kiehl, W. M. Washington, Q. Fu, D. R. Sikka and M. Wild, *Proc. Natl. Acad. Sci. U. S. A.*, 2005, **102**, 5326–5333.

61 W. S. Drysdale, PhD thesis, University of York, 2020.

62 B. S. Nelson, D. J. Bryant, M. S. Alam, R. Sommariva, W. J. Bloss, M. J. Newland, W. S. Drysdale, A. R. Vaughan, W. J. F. Acton, C. N. Hewitt, L. R. Crilley, S. J. Swift, P. M. Edwards, A. C. Lewis, B. Langford, E. Nemitz, Shivani, R. Gadi, B. R. Gurjar, D. E. Heard, L. K. Whalley, Ü. A. Şahin, D. C. S. Beddows, J. R. Hopkins, J. D. Lee, A. R. Rickard and J. F. Hamilton, Extreme Concentrations of Nitric Oxide Control Daytime Oxidation and Quench Nocturnal Oxidation Chemistry in Delhi during Highly Polluted Episodes, *Environ. Sci. Technol. Lett.*, 2023, **10**, 520–527.

 © 2025 The Author(s). Published by the Royal Society of Chemistry